Silicone implant surface roughness, friction, and wear

Surface Topography: Metrology and Properties

PAPER

Silicone implant surface roughness, friction, and wear

Dixon J Atkins[1], **Allison L Chau**[2], **Jonah M Rosas**[1], **Yen-Tsung Chen**[3], **Samantha T Chan**[4], **Juan Manuel Urueña**[5] and **Angela A Pitenis**[2]

[1] Department of Biomolecular Science and Engineering, University of California, Santa Barbara, United States of America
[2] Materials Department, University of California, Santa Barbara, United States of America
[3] Department of Chemical Engineering, University of California, Santa Barbara, United States of America
[4] Department of Molecular, Cellular, and Developmental Biology, University of California, Santa Barbara, United States of America
[5] NSF BioPACIFIC Materials Innovation Platform, University of California, Santa Barbara, United States of America

E-mail: apitenis@ucsb.edu

Keywords: tribology, debris, friction, surface roughness

Supplementary material for this article is available online

OPEN ACCESS

RECEIVED
2 February 2022

REVISED
29 September 2022

ACCEPTED FOR PUBLICATION
2 November 2022

PUBLISHED
20 March 2023

Abstract

Some textured silicone breast implants with high average surface roughness ('macrotextured') have been associated with a rare cancer of the immune system, Breast Implant-Associated Anaplastic Large Cell Lymphoma (BIA-ALCL). Silicone elastomer wear debris may lead to chronic inflammation, a key step in the development of this cancer. Here, we model the generation and release of silicone wear debris in the case of a folded implant-implant ('shell-shell') sliding interface for three different types of implants, characterized by their surface roughness. The 'smooth' implant shell with the lowest average surface roughness tested ($R_a = 2.7 \pm 0.6$ μm) resulted in average friction coefficients of $\mu_{avg} = 0.46 \pm 0.11$ across 1,000 mm of sliding distance and generated 1,304 particles with an average particle diameter of $D_{avg} = 8.3 \pm 13.1$ μm. The 'microtextured' implant shell ($R_a = 32 \pm 7.0$ μm) exhibited $\mu_{avg} = 1.20 \pm 0.10$ and generated 2,730 particles with $D_{avg} = 4.7 \pm 9.1$ μm. The 'macrotextured' implant shell ($R_a = 80 \pm 10$ μm) exhibited the highest friction coefficients, $\mu_{avg} = 2.82 \pm 0.15$ and the greatest number of wear debris particles, 11,699, with an average particle size of $D_{avg} = 5.3 \pm 3.3$ μm. Our data may provide guidance for the design of silicone breast implants with lower surface roughness, lower friction, and smaller quantities of wear debris.

1. Introduction

Silicone elastomer materials are considered the 'gold standard' for long-term medical devices designed to restore proper function or adjust form, including shunts, ports, drains, biosensors, and prostheses. Some of the most common silicone elastomer implants are used annually for breast augmentation (2 million) and reconstruction (>100,000) surgeries, and silicone breast implants have been used for these operations for the last six decades [1–3]. Silicone elastomers are frequently leveraged in biomedical applications due to their thermal and chemical stability, tunable mechanical properties, and perceived biocompatibility [4]. However, there is no such thing as a biocompatible material [5]. Certain silicone elastomer implants have been linked to adverse conditions, including chronic inflammation [6], capsular contracture, and in rare instances, cancer. Silicone granulomas around breast implants have been increasingly diagnosed since the early 2000s [7, 8] and breast-implant anaplastic large-cell lymphoma (BIA-ALCL) has been associated with silicone breast implant shells with aggressive surface texturing [9–14]. Once shed, non-biodegradable silicone wear debris particulates may perpetually provoke the immune response [15–18]. As cytokines and pro-inflammatory markers accumulate around wear debris particles, reactive oxygen species and continued inflammation may damage increasingly larger areas of tissue. Silicone elastomer particulates [19] and immune cells [6] have been discovered in fibrous capsules retrieved from patients, which supported the long-standing hypothesis that implant wear debris may initiate the pro-inflammatory immune response and lead to adverse conditions [10, 20].

In an effort to mitigate the risks of implant debris, international standards require, '*both inside and*

outside of the shell shall be suitable to minimize frictional abrasion between shell-to-shell surface and between shell surface and the implantation site' (ISO 14 607:2018) [21]. Additionally, new European Union regulations on medical devices requires, '*devices shall be designed and manufactured in such a way as to reduce as far as possible the risks posed by substances or particles, including wear debris, degradation products and processing residues, that may be released from the device.*' [22] Despite these mandates, the tribological mechanisms by which silicone elastomer wear debris is generated and released into the breast pocket is highly complex and poorly understood. Frustrating fundamental studies of elastomer friction and wear are challenges posed by the coupled contributions of implant surface roughness, thickness, elastic modulus, and viscoelasticity. While most commercially-available silicone elastomers used for breast implant shells generally share similar mechanical properties, their exterior surface texture may vary by several orders of magnitude. In this work, we investigate likely tribological conditions for wear debris particulates to form *in vivo*: those occurring during patient reports of implant 'wrinkling', 'rippling', 'folding'; essentially, any sliding contact across the shell-to-shell interface. Here, we conduct an *in vitro* investigation of the tribological mechanisms of wear debris formation associated with silicone elastomer breast implants with varying magnitudes of surface roughness. We examine ISO14607:2018-designated 'smooth' ($R_a < 10$ μm), 'microtextured' (10 μm $< R_a <$ 50 μm), and 'macrotextured' ($R_a > 50$ μm) implant surfaces to investigate the relationships between surface roughness, friction, and wear debris formation and the potential links to soft tissue damage and disease [21].

2. Materials and methods

2.1. Implant surface characterization

Section of unused and de-gelled commercially-available silicone breast implant shells, Allergan® Smooth ($R_a = 0.2 \pm 0.03$ μm), Motiva® Ergonomix® SmoothSilk® ($R_a = 2.7 \pm 0.6$ μm), Mentor® Siltex® ($R_a = 32 \pm 7.0$ μm), and Allergan® BioCell® ($R_a = 80 \pm 10.0$ μm) were used to model the dynamic sliding interface of a folded breast implant surface. The Allergan® BioCell® 'macrotextured' implant in this study was voluntarily recalled by the manufacturer in 2019 due to its association with a rare lymphoma [23, 24]. For the remainder of the text, we will refer to each breast implant surface by its average surface roughness value, R_a. Representative (6 mm diameter) sections of the $R_a = 0.2$ μm, $R_a = 2.7$ μm, and $R_a = 32$ μm breast implant shells were examined using scanning electron microscopy (SEM, FEI Nova Nano 650 FEG SEM) and 3D laser confocal scanning microscopy (Keyence VK-X3000) as reported in 25. Implant shell sections were subsequently cut into thin strips (2 mm width, 6 mm length) with a sharp blade and imaged in cross-section using SEM to acquire high-resolution micrographs of the surface topography in direct sliding contact with soft tissues. Schematic representations of the implant-implant interface based on SEM micrographs are shown in figures 1(b)–(e). The average surface roughness, R_a, of the breast implant shells $R_a = 0.2$ μm, $R_a = 2.7$ μm, and $R_a = 32$ μm were measured with the 3D surface profiler across a roughly 700 $\times$ 500 μm region from at least 20 line scans. Surface roughness characterization of the macrotextured breast implant surface $R_a = 80$ μm is reported in references [26] and [27]. Additional surface roughness parameters for each breast implant sample are compiled in supplementary table S1.

2.2. Power spectral density calculation

Line scan traces of each implant's surface profile were taken from cross-sections of scanning electron micrographs (see supplementary figure S1) and converted into vector form. Power spectra were calculated using the Matplotlib library in Python and Welch's average periodogram method [28]. Data for the line scans are compiled in supplementary tables S2a-d.

2.3. Implant probe preparation and assembly

Sections of silicone breast implant shells (6 mm radius) were mounted with cyanoacrylate adhesive on hydrogel probes with spherical shell geometries (previously described in [29]). Poly(hydroxyethyl)methacrylate (pHEMA) shell probes (6 mm radius of curvature, 300 μm apical thickness) were prepared by combining 67 wt.% 2-hydroxyethyl methacrylate (HEMA), 0.2 wt.% MBAm, 0.15 wt.% TEMED, 0.15 wt.% APS, and ultrapure water. Hydrogel shell probes were polymerized in custom polyoxymethylene molds, heated to 60 °C for 1 h and then equilibrated in ultrapure water for at least 24 h. A polyethylene collar was fitted around the silicone elastomer implant shell section and pHEMA probe to mitigate slip during sliding experiments. A more detailed schematic of the probe design can be found in Supplementary figure S3.

2.4. In situ microtribometer

Tribological testing was conducted in a soft-walled clean room. Experiments were performed using a custom linear reciprocating microtribometer mounted to the condenser turret of an inverted laser scanning confocal microscope (Nikon A1R HD) previously described in [30]. The implant probe assembly was fastened to a titanium double-leaf cantilever flexure with normal and tangential stiffnesses of $k_n = 225$ μN/μm and $k_t = 122$ μN/μm, respectively. Capacitance sensors (Lion Precision, sensitivity:

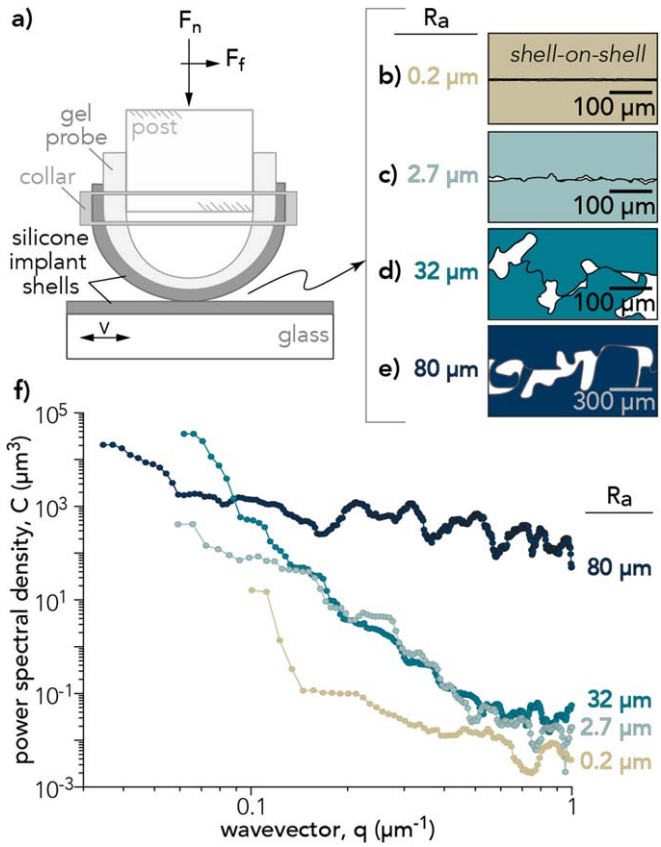

Figure 1. (a) Illustration of tribometer configuration. Implant surfaces (10 mm radius) were secured to glass-bottomed culture dishes and to hydrogel probes with spherical shell geometry (6 mm radius of curvature) and fully submerged in ultrapure water to investigate shell-shell tribological interactions. (b–e) Representative traces of implant surface profiles measured by scanning electron microscopy: $R_a = 0.2$ μm (tan); $R_a = 2.7$ μm (light green); $R_a = 32$ μm (teal); $R_a = 80$ μm (navy). Line scans illustrate prominent surface features that may interact in a folded implant scenario. f) One-dimensional power spectral density curves showing surface topography for silicone implants with $R_a = 0.2$ μm (tan); $R_a = 2.7$ μm (light green); $R_a = 32$ μm (teal); $R_a = 80$ μm (navy) using the SEM traces of implant surface profiles in (b–e).

5 μm/V, range: 20 V) measured cantilever displacements in the normal and tangential directions, which were converted to normal and friction forces using a custom LabVIEW program. The measurement uncertainties in normal force and friction force were $u(F_n) = \pm 2$ μN and $u(F_f) = \pm 1$ μN, respectively. Silicone elastomer breast implant shell surfaces were ultrasonicated in water for 20 min at 37 kHz and allowed to evaporate under dry nitrogen. This process was repeated twice, after which no debris particles were detected in the supernatant. Cleaned silicone elastomer samples were stored in a dust-free sterile environment until testing. The cleaned silicone implant shell surfaces were loaded into opposing contact (shell-to-shell) and subjected to dynamic sliding conditions (1 mN normal force, 1 mm s^{-1} sliding velocity, 5 mm sliding path length) while fully submerged in ultrapure water to simulate probable tribological interactions experienced during implant folding events.

For each sliding cycle, friction coefficients (μ_{cycle}) were calculated by dividing the average friction force (over the forward, $F_{f_{fwd}}$, and reverse, $F_{f_{rev}}$, directions) by the average normal force (F_n) within the free sliding regime (middle 25% of the sliding path) (equation (1)).

$$\mu_{cycle} = \frac{\langle F_{f_{fwd}} \rangle - \langle F_{f_{rev}} \rangle}{2\langle F_n \rangle} \quad (1)$$

2.5. Wear debris collection and analyses

Following tribological testing, debris particle quantity and size were determined by ultrasonicating at 37 kHz both implant surfaces of the shell-to-shell sliding contact for 20 min in 12 ml of ultrapure water (Fisherbrand Advanced Ultrasonic Cleaner, model FB11201). Solutions were vigorously pipette-mixed and transferred into 15 ml centrifuge tubes and centrifuged at 3,200 g for 15 min and slowly decelerated. Supernatant was removed, debris particles were resuspended with a vortex mixer, and 20 μl of the concentrated particle solutions were pipetted onto glass slides and covered with glass coverslips. Debris particles dried for at least 24 h in a sterile environment before imaging.

3. Results and discussion

The material and tribological properties of soft silicone breast implants were evaluated to examine the role of

surface roughness on damage to these implants under dynamic sliding conditions. Figure 1(a) shows a schematic of the tribometer configuration. Silicone implant shells were brought into self-mating contact between a glass bottom culture dish and a hydrogel membrane probe. The implant section adhered to the gel probe was secured using a custom-fit polyethylene collar. Figures 1(b)–(e) compare the surface topography of breast implants from cross-sectional SEM micrographs converted into two-dimensional traces. Distinct and representative features of each silicone breast implant surface have been shown to highlight key differences in the surface roughness, R_a. The 1D power spectral density (PSD) curves, shown in figure 1(f), demonstrate surface roughness feature amplitudes as a function of the spatial frequency. PSD curves encode key surface roughness measurements; the root mean square (RMS) roughness of the sample is the square root of the sum of the power spectrum (total power). Rougher samples have higher total power, and flatter samples are likely to have fewer spectral spikes.

3.1. Tribological measurements

Three individual shell-on-shell sliding experiments were conducted to investigate the relationships between roughness, friction, and wear of elastomers. New probes and countersamples were used for each of the three implant surfaces tested for a total of nine experiments overall. Representative friction force traces as a function of position for silicone implants tested in a shell-on-shell sliding configuration are shown in figure 2(a). Increasing surface roughness increased the friction force across the shell-shell interface under the same nominal normal force (1 mN). The friction coefficient, μ, was analyzed across the middle 25% of the sliding path and generally increased with increasing sliding distance, as shown in figure 2(b). The 'smooth' implant ($R_a = 2.7$ μm) exhibited initial sliding friction coefficients of about $\mu \approx 0.1$ for the first 200 mm of travel and gradually increased to about $\mu \approx 0.5$ for the remainder of the experiment. The 'microtextured' implant ($R_a = 32$ μm) remained near $\mu \approx 1.2$ for the duration of the experiment, with the exception of a sudden drop after the first few cycles. One potential explanation for the transient drop in friction coefficient seen in the $R_a = 32$ μm sample from 20 mm to 40 mm of sliding (equivalent to reciprocating cycles 2 and 3) in figure 2(b) may be transient run-in of the highest asperities, seen in figure 1(d). The 'macrotextured' implant ($R_a = 80$ μm) exhibited initial friction coefficients near $\mu \approx 1.9$ and steadily increased to $\mu \approx 2.4$. Dynamic changes in friction coefficient measurements are well-aligned with our observations of wear debris collected after 10, 100, and 1,000 cycles, which indicate that the majority of debris is generated within the first 100 cycles (1,000 mm total sliding distance). Tribological testing revealed that increasing surface roughness of silicone implants resulted in increased average friction coefficients across the shell-shell sliding interface (figure 2(c)). This is perhaps surprising given that the real area of contact should decrease with increasing surface roughness. While we could not measure the real area of contact during these studies, we postulate that the flexibility and elasticity of the cone-like asperities distributed across the surfaces of the silicone elastomer shells, particularly for the 'microtextured' ($R_a = 32$ μm) and 'macrotextured' ($R_a = 80$ μm) implants, may have contributed to increased asperity-asperity interactions and ultimately greater friction coefficients. We also examined silicone breast implant shells with surface roughness $R_a = 0.2$ μm, but the adhesive forces across this smooth and flat interface prohibited free sliding.

3.2. Image analysis

Image analyses revealed that increasing surface roughness increased the quantity of wear debris particles shed during shell-on-shell sliding experiments. The 'macrotextured' implant surface $R_a = 80$ μm shed roughly five times the quantity of wear debris particles (total: 11,699 particles) compared to the 'microtextured' surface, with average surface roughness $R_a = 32$ μm (total: 2,730 particles). The total number of wear debris particles shed from the $R_a = 2.7$ μm was 1,304. The wear debris particle counts reported herein are each from a single shell-on-shell sliding experiment for every implant surface.

The average and standard deviation of wear debris particle diameters shed from implant surfaces $R_a = 32$ μm and $R_a = 80$ μm were 4.7 ± 9.1 μm and 5.3 ± 3.3 μm, respectively (figure 3(a)). These values lie within the optimal range of macrophage phagocytosis, typically between 1 and 15 μm [19, 31]. Macrophages are approximately 20 μm in diameter and struggle to phagocytose particles larger than 20 μm. The average wear debris particle diameter of the 'smooth' implant surfaces was 8.3 ± 13.1 μm. Representative images of wear debris particles diluted to 0.5% concentration (v/v %) are shown in figures 3(b)–(d). These results suggest that implants with higher surface roughness may generate more wear debris particles during shell-shell sliding events and that those shed particles are more likely to have size distributions within the optimal range of macrophage phagocytosis.

The minimum detectable particle diameter using the methods described herein was 1.5 μm. Efforts to accurately identify individual wear debris particles were frustrated by occasional agglomerations of several particles. Thus, the debris collected, analyzed, and reported herein likely does not represent all the particles generated across the sliding interface and may underestimate the *in vivo*

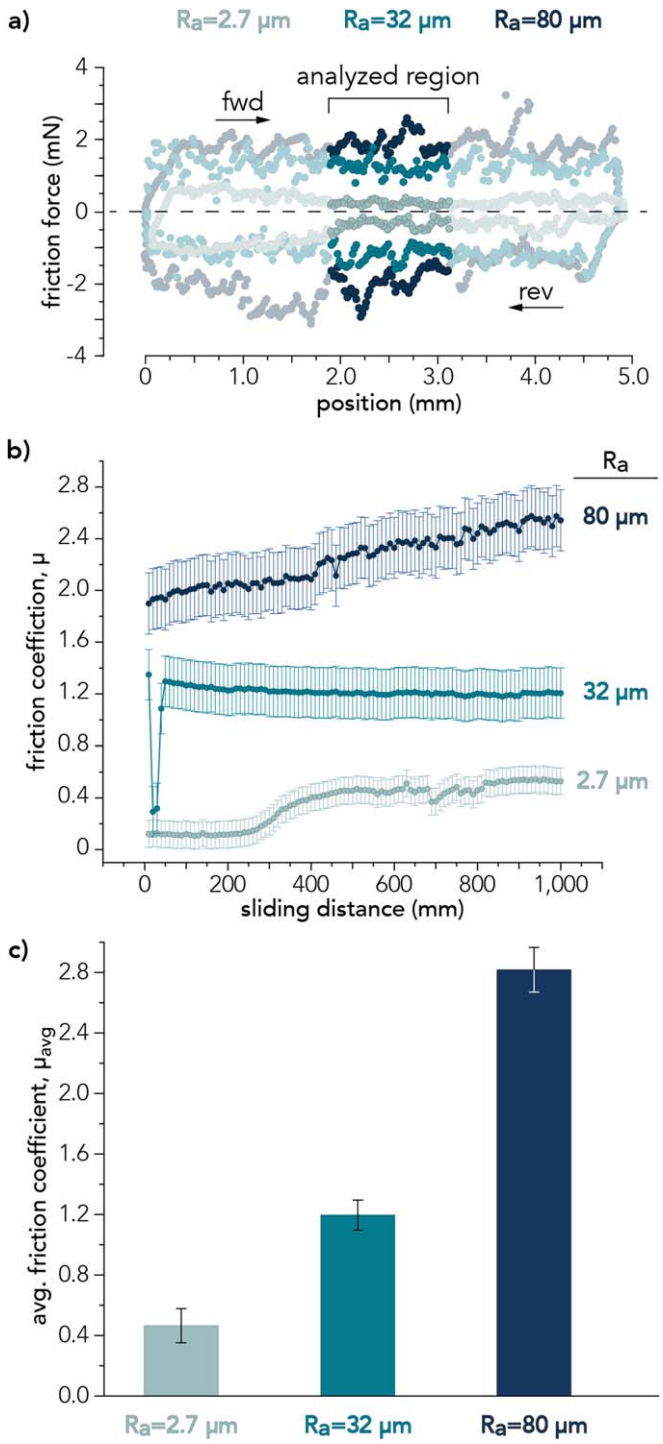

Figure 2. (a) Friction force trace of a single reciprocating cycle for three breast implant shell samples of $R_a = 2.7$ μm (light green); 32 μm (teal); 80 μm (navy) sliding against a 20 mm diameter disk of the same implant surface (shell-on-shell sliding configuration). Experimental conditions: normal load, $F_n = 1$ mN; sliding speed, $v = 0.5$ mm s^{-1}; sliding path length, $l = 5$ mm (1/2 cycle). For each sliding cycle, friction force and friction coefficients were averaged across the middle 25% of the sliding path, within the free sliding regime. b) Friction coefficients of breast implant surfaces as a function of sliding distance. Friction coefficients were calculated using equation (1). Error bars represent the standard deviation across the middle 25% of the sliding path for one reciprocating cycle. c) Friction coefficients of silicone breast implant surfaces averaged over $n = 100$ cycles for three individual experiments resulted in: $\mu_{avg} = 0.46 \pm 0.11$ for $R_a = 2.7$ μm (light green); $\mu_{avg} = 1.20 \pm 0.10$ for $R_a = 32$ μm (teal); and $\mu_{avg} = 2.82 \pm 0.15$ for $R_a = 80$ μm (navy). Error bars represent the standard deviation in friction coefficients across three individual shell-on-shell sliding experiments.

availability of silicone elastomer debris particles. The silicone breast implant surfaces were observed before and after sliding using scanning electron microscopy as well as an inverted laser scanning confocal microscopy (Nikon A1R HD) and the autofluorescent properties of the silicone elastomer breast implant samples under 488 nm of light after 1,000 mm of sliding. Despite clear evidence of wear debris, there was no discernible 'smoothing' of the breast implant surface for any samples tested.

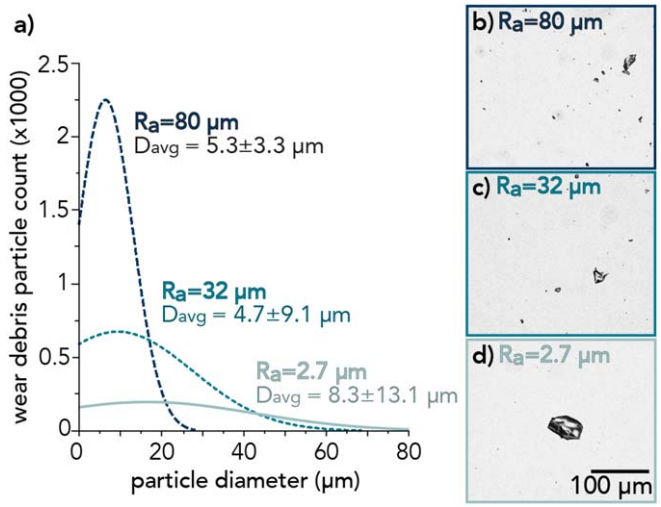

Figure 3. a) Distribution curves of the quantity and diameter of silicone elastomer breast implant wear debris particles generated after 1,000 mm of sliding in shell-on-shell configurations. Average particle diameter and standard deviation for implants with surface roughness: 8.3 ± 13.1 μm for $R_a = 2.7$ μm (solid light green); 4.7 ± 9.1 μm for $R_a = 32$ μm (dotted teal); 5.3 ± 3.3 μm for $R_a = 80$ μm (dashed navy). Representative widefield images under 40x magnification of implant wear debris particles diluted to 0.5% concentration of total particle volume in ultrapure water for b) $R_a = 80$ μm, c) $R_a = 32$ μm, and d) $R_a = 2.7$ μm.

Table 1. Average surface roughness, R_a, wear debris particle diameter, D_{avg}, particle count, volume loss, V_{loss}, and wear rate, K after 1,000 mm of shell-on-shell sliding with $R_a = 2.7$ μm, $R_a = 32$ μm, and $R_a = 80$ μm silicone elastomer implant shells. The $R_a = 0.2$ μm shell-on-shell sliding experiment could not be conducted due to excessively high adhesion between the smooth and flat surfaces.

R_a (μm)	D_{avg} (μm)	count	V_{loss} (mm^3)	K (mm^3/N·m)
0.2 ± 0.03	----	----	----	----
2.7 ± 0.6	8.3 ± 13.1	1,304	8×10^{-2}	8×10^{-5}
32 ± 7.0	4.7 ± 9.1	2,730	10×10^{-2}	10×10^{-5}
80 ± 10.0	5.3 ± 3.3	11,699	5×10^{-2}	5×10^{-5}

3.3. Wear rate calculations

Wear rates of the implant-implant sliding interactions were calculated by dividing the total volume loss (V_{loss}) by the average normal force (F_n) multiplied by the sliding distance (d) (equation (2)). Volume loss was approximated using wear debris particle diameter and assuming spherical particle geometry.

$$K = \frac{V_{loss}}{F_n \cdot d} \tag{2}$$

Each sample experienced an average normal force of 1 mN across 1,000 mm of sliding distance. Wear rates of these silicone implant samples were calculated to be $8 \times 10^{-5} \frac{mm^3}{N \cdot m}$, $10 \times 10^{-5} \frac{mm^3}{N \cdot m}$, and $5 \times 10^{-5} \frac{mm^3}{N \cdot m}$ for $R_a = 2.7$ μm, $R_a = 32$ μm, and $R_a = 80$ μm, respectively. These values are reported in table 1, along with the average volume of debris shed and the average diameter of the debris particles. The total volume of debris particles was estimated by the considering spherical shape of particles with the distribution shown in figure 3(a). The calculated wear rates fall within an order of magnitude of previously reported wear rates of elastomers [32].

4. Conclusions

In this investigation, we examined the extent to which the surface roughness of silicone breast implant shells induces debris formation in an implant-implant sliding interface that models a folded breast implant. 'Smooth' silicone elastomer breast implants in self-mated sliding configurations (shell-to-shell) ($R_a < 10$ μm) resulted in the lowest friction coefficients ($\mu \approx 0.5$) and the fewest wear debris particles in the size range favored by macrophages (1 to 15 μm particle diameter). 'Microtextured' silicone elastomer breast implants in shell-to-shell sliding contact (10 μm $< R_a < 50$ μm) resulted in higher friction coefficients ($\mu \approx 1$) and generated moderate amounts of small wear debris particles. However, 'macrotextured' silicone

elastomer breast implants in shell-to-shell sliding contact ($R_a > 50$ μm) resulted in the highest friction coefficients ($\mu > 2$) and the highest quantity of the smallest debris particles. In contrast, self-mated sliding contact was precluded for the smoothest implant surface, ($R_a = 0.2$ μm), due to extremely high adhesion. These findings highlight the importance of designing silicone elastomer breast implant shells within an optimal range of surface roughness to reduce frictional shear stresses and wear debris generation during shell-to-shell tribological interactions.

Acknowledgments

We thank Megan Cavanaugh and Andrew Bordeos for valuable discussions and assistance in materials characterization. The use of the shared facilities of the National Science Foundation (NSF) Materials Research Science and Engineering Center (MRSEC) at UC Santa Barbara is gratefully acknowledged; the UCSB MRSEC is a member of the Materials Research Facilities Network (www.mrfn.org). This work was supported by the BioPACIFIC Materials Innovation Platform of the National Science Foundation under Award No. DMR-1933487.

Data availability statement

The data that support the findings of this study are available upon reasonable request from the authors.

Declaration of conflicting interests

The authors declare no competing interests.

Funding

This work was partially supported by the National Science Foundation (NSF) Materials Research Science and Engineering Center (MRSEC) at UC Santa Barbara under Award No. DMR-1720256 (IRG-3). This work was partially supported by Establishment Labs, Costa Rica. Establishment Labs did not take part in the study design, collection or analysis of the data; in writing the journal article, or the decision to submit for publication. D.J.A. acknowledges support by the National Institute of General Medical Sciences of the National Institutes of Health under Award No. T32GM141846. A.L.C. acknowledges support of the National Science Foundation Graduate Research Fellowship Program under Grant No. 1 650 114. J.M.R. acknowledges support from the Gates Millennium Scholarship through the Bill and Melinda Gates Foundation and Hispanic Scholarship Fund.

ORCID iDs

Dixon J Atkins https://orcid.org/0000-0002-8871-4037
Allison L Chau https://orcid.org/0000-0003-4435-8373
Jonah M Rosas https://orcid.org/0000-0001-7754-7002
Yen-Tsung Chen https://orcid.org/0000-0002-7444-5518
Angela A Pitenis https://orcid.org/0000-0002-9697-7291

References

[1] Jalalabadi F, Doval A F, Neese V, Andrews E and Spiegel A J 2021 Breast implant utilization trends in usa versus europe and the impact of bia-alcl publications *Plastic and Reconstructive Surgery -Global Open* **9** e3449
[2] Beekman W H, Hage J J, Jorna L B and Mulder J W 1999 Augmentation mammaplasty: the story before the silicone bag prosthesis *Ann Plast Surg* **43** 446–51
[3] Saldanha I J, Broyles J M, Adam G P, Cao W, Bhuma M R, Mehta S, Pusic A L, Dominici L S and Balk E M 2022 Implant-based breast reconstruction after mastectomy for breast cancer: a systematic review and meta-analysis *Plast Reconstr Surg Glob Open* **10** e4179
[4] Curtis J and Steichen S D 2020 1.3.2b—silicones *Biomaterials Science* ed W R Wagner *et al* 4th edn (New York: Academic) pp 109–23
[5] Williams D F 2014 There is no such thing as a biocompatible material *Biomaterials* **35** 10009–14
[6] Wolfram D, Rainer C, Niederegger H, Piza H and Wick G 2004 Cellular and molecular composition of fibrous capsules formed around silicone breast implants with special focus on local immune reactions *J Autoimmun* **23** 81–91
[7] Austad E D 2002 Breast implant-related silicone granulomas: the literature and the litigation *Plast Reconstr Surg* **109** 1724–30
[8] Park M E, Curreri A T, Taylor G A and Burris K 2016 Silicone granulomas, a growing problem? *The Journal of Clinical and Aesthetic Dermatology* **9** 48–51
[9] Hallab N J and Jacobs J J 2009 Biologic effects of implant debris *Bull NYU Hosp Jt Dis* **67** 182–8
[10] Hallab N J, Samelko L and Hammond D 2019 The inflammatory effects of breast implant particulate shedding: comparison with orthopedic implants *Aesthetic Surgery Journal* **39** S36–48
[11] Manikkam Umakanthan J, McBride C L, Greiner T, Yuan J, Sanmann J, Bierman P J, Lunning M A and Bociek R G 2017 Bariatric implant-associated anaplastic large-cell lymphoma *Journal of Oncology Practice* **13** 838–9
[12] DeCoster R C, Clemens M W, Di Napoli A, Lynch E B, Bonaroti A R, Rinker B D, Butterfield T A and Vasconez H C 2021 Cellular and molecular mechanisms of breast implant-associated anaplastic large cell lymphoma *Plastic and Reconstructive Surgery* **147** 30e-41e
[13] Doren E L, Miranda R N, Selber J C, Garvey P B, Liu J, Medeiros L J, Butler C E and Clemens M W 2017 U.S. epidemiology of breast implant-associated anaplastic large cell lymphoma *Plastic and Reconstructive Surgery* **139** 1042–50
[14] Shauly O, Gould D J, Siddiqi I, Patel K M and Carey J 2019 The First Reported Case of Gluteal Implant-Associated Anaplastic Large Cell Lymphoma (ALCL) *Aesthetic Surgery Journal* **39** NP253–NP258
[15] Webb L H, Aime V L, Do A, Mossman K and Mahabir R C 2017 Textured breast implants: a closer look at the surface debris under the microscope *Plastic surgery (Oakville, Ont.)* **25** 179–83

[16] Katzin W E, Feng L J, Abbuhl M and Klein M A 1996 Phenotype of lymphocytes associated with the inflammatory reaction to silicone gel breast implants *Clin Diagn Lab Immunol* **3** 156–61
[17] de Faria Castro Fleury E, Gianini A C, Ayres V, Ramalho L C, Seleti R O and Roveda D J 2017 Breast magnetic resonance imaging: tips for the diagnosis of silicone-induced granuloma of a breast implant capsule (sigbic) *Insights Imaging* **8** 439–46
[18] Hallab N J, Cunningham B W and Jacobs J J 2003 Spinal implant debris-induced osteolysis *Spine (Phila Pa 1976)* **28** S125–38
[19] Hallab N J, Samelko L and Hammond D 2021 Particulate debris released from breast implant surfaces is highly dependent on implant type *Aesthet Surg J* **41** NP782–NP793
[20] Charnley J 1970 The reaction of bone to self-curing acrylic cement. a long-term histological study in man *J Bone Joint Surg Br* **52** 340–53
[21] ISO14607:2018: Non-active surgical implants - Mammary implants - Particular requirements https://www.iso.org/obp/ui/#iso:std:iso:14607:ed-3:v2:en
[22] Regulation (eu) 2017/745 of the european parliament and of the council of 5 april 2017 on medical devices, amending directive 2001/83/ec, regulation (ec) no 178/2002 and regulation (ec) no 1223/2009 and repealing council directives 90/385/eec and 93/42/eec
[23] Swanson E 2019 Plastic surgeons defend textured breast implants at 2019 U.S. food and drug administration hearing: why it is time to reconsider *Plast Reconstr Surg Glob Open* **7** e2410
[24] Dowson D 2012 Bio-tribology *Faraday Discuss* **156** 9–30
[25] Rosas J M, Atkins D J, Chau A L, Chen Y-T, Bae R, Cavanaugh M K, Espinosa Lima R I, Bordeos A, Bryant M G and Pitenis A A 2022 *In vitro* models of soft tissue damage by implant-associated frictional shear stresses *Proc. Inst. Mech. Eng. J* **OnlineFirst** 1–8
[26] Atlan M, Nuti G, Wang H, Decker S and Perry T 2018 Breast implant surface texture impacts host tissue response *J. Mech. Behav. Biomed. Mater.* **88** 377–85
[27] Munhoz A M, Clemens M W and Nahabedian M Y 2019 Breast implant surfaces and their impact on current practices: where we are now and where are we going? *Global Open* **7** e2466
[28] Hunter J D 2007 Matplotlib: a 2d graphics environment *Comput. Sci. Eng.* **9** 90–5
[29] Marshall S L, Schulze K D, Hart S M, Uruea J M, McGhee E O, Bennett A I, Pitenis A A, O'Bryan C S, Angelini T E and Sawyer W G 2017 Spherically capped membrane probes for low contact pressure tribology *Biotribology* **11** 69–72 Special issue on the III International Conference on Biotribology
[30] Urueña J M, Hart S M, Hood D L, McGhee E O, Niemi S R, Schulze K D, Levings P P, Sawyer W G and Pitenis A A 2018 Considerations for biotribometers: Cells, gels, and tissues *Tribol. Lett.* **66** 141
[31] Baranov M V, Kumar M, Sacanna S, Thutupalli S and van den Bogaart G 2021 Modulation of immune responses by particle size and shape *Frontiers in Immunology* **11** 45
[32] Rowe K G, Bennett A I and Sawyer W G 2016 Traction and wear of an elastomer in combined rolling and sliding *Lubr. Sci.* **28** 97–106